

Large-Scale Power Spectrum and Structures From the ENEAR galaxy Peculiar Velocity Catalog

S. Zaroubi¹, M. Bernardi^{1,2,3}, L.N. da Costa^{2,4}, Y. Hoffman⁵, V. Alonso⁶,
G. Wegner⁷, C.N.A. Willmer^{4,8}, P.S. Pellegrini⁴

¹Max Planck Institut für Astrophysik, Karl-Schwarzschild-Str. 1, 85748 Garching, Germany.

²European Southern Observatory, Karl-Schwarzschild-Str. 2, 85748 Garching, Germany.

³Universitäts-Sternwarte München, Scheiner-Str. 1, D-81679 München, Germany.

⁴Observatório Nacional, Rua General José Cristino 77, Rio de Janeiro, R. J. 20921 Brazil.

⁵Racah Institute of Physics, The Hebrew University, Jerusalem 91904, Israel.

⁶Observatorio Astronómico de Córdoba Laprida 854, Córdoba (5000), Argentina.

⁷Department of Physics and Astronomy, 6127 Wilder Laboratory, Dartmouth College, Hanover, NH 03755-3528.

⁸UCO/Lick Observatory, University of California, 1156 High Street, Santa Cruz, CA 95064

25 October 2018

ABSTRACT

We estimate the *mass* density fluctuations power spectrum (PS) on large scales by applying a maximum likelihood technique to the peculiar velocity data of the recently completed redshift-distance survey of early-type galaxies (hereafter ENEAR). Parametric CDM-like models for the PS are assumed, and the best fit parameters are determined by maximizing the probability of the model given the measured peculiar velocities of the galaxies, their distances and estimated errors. The method has been applied to CDM models with and without COBE normalization. The general results are in agreement with the high amplitude power spectra found from similar analysis of other independent all-sky catalogs of peculiar velocity data such as MARK III (Willick *et al.* 1997) and SFI (Giovanelli *et al.* 1998; da Costa *et al.* 1996), in spite of the differences in the way these samples were selected, the fact that they probe different regions of space and galaxy distances are computed using different distance relations. For example, at $k = 0.1 h \text{ Mpc}^{-1}$ the power spectrum value is $P(k)\Omega^{1.2} = (6.5 \pm 3) \times 10^3 (h^{-1} \text{ Mpc})^3$ and $\eta_8 \equiv \sigma_8 \Omega^{0.6} = 1.1^{+0.2}_{-0.35}$; the quoted uncertainties refer to 3σ error level. We also find that, for Λ CDM and OCDM COBE-normalized models, the best-fit parameters are confined by a contour approximately defined by $\Omega h^{1.3} = 0.377 \pm 0.08$ and $\Omega h^{0.88} = 0.517 \pm 0.083$ respectively. Γ -shape models, free of COBE normalization, results in the weak constraint of $\Gamma \geq 0.17$ and in the rather stringent constraint of $\eta_8 = 1.0 \pm 0.25$. All quoted uncertainties refer to 3σ confidence-level (*c.l.*).

The calculated PS has been used as a prior for Wiener reconstruction of the density field at different resolutions and the three-dimensional velocity field within a volume of radius $\approx 80 h^{-1} \text{ Mpc}$. All major structures in the nearby universe are recovered and are well matched to those predicted from all-sky redshift surveys. The robustness of these features has been tested with Constrained Realizations (CR). Analysis of reconstructed three-dimensional velocity field yields a small bulk flow amplitude ($\sim 160 \pm 60 \text{ km s}^{-1}$ at $60 h^{-1} \text{ Mpc}$) and a very small rms value of the tidal field ($\sim 60 \text{ km s}^{-1}$). The results give further support to the picture that most of the motion of the Local Group arises from mass fluctuations within the volume considered.

Key words: cosmology: observations – cosmology: theory – dark matter – galaxies: distances and redshifts – large-scale structure of universe – methods: statistical

1 INTRODUCTION

The canonical model of cosmology assumes that large-scale structure has grown out of small density perturbations via

arXiv:astro-ph/0005558v1 29 May 2000

the process of gravitational instability. These initial fluctuations are usually assumed to satisfy the statistics of a Gaussian random field, solely characterized by its power spectrum. In the linear regime, the fluctuations grow self-similarly and retain their initial distribution and power spectrum shape. Therefore, mapping the underlying cosmological velocity field and its power spectrum on large scales, provides a direct probe to the origin of structure in the universe.

The PS, the three-dimensional distribution of luminous matter and the predicted peculiar velocity field have been derived from a variety of data sets, especially from all-sky redshift surveys (*e.g.* Strauss & Willick 1995 for a review of earlier work; Sutherland *et al.* 1999; Branchini *et al.* 1999). Unfortunately, however, the distribution of galaxies in these catalogs is not necessarily an unbiased tracer of the underlying mass distribution, and suffer from the infamous “galaxy biasing” problem. Furthermore, in estimates from redshift surveys, uncertainties arise from the complicated relation between the real space and the redshift space distributions, known as redshift distortions (*e.g.*, Kaiser 1987, Zaroubi and Hoffman 1996). In order to avoid these problems altogether it is advantageous to appeal to dynamical data, in particular catalogs of galaxy peculiar velocities on large scales.

Peculiar velocities enable a direct and reliable determination of the mass PS and distribution, under the natural assumption that the galaxies are unbiased tracers of the large-scale, gravitationally-induced, velocity field. Furthermore, since peculiar velocities are non-local and have contributions from different scales, analysis of the peculiar velocity field provides information on scales somewhat larger than the sampled region (*e.g.* Hoffman *et al.* 2000). For the same reason peculiar velocities are adequately described by linear theory even when densities become quasi-linear (*e.g.*, Freudling *et al.* 1999). Consequently, the dynamics and the distribution of peculiar velocities are well described by the linear regime of gravitational instability and by a Gaussian probability distribution function (PDF), respectively.

Assuming that both the underlying velocity field and the errors are drawn from independent random Gaussian fields, the observed peculiar velocities constitute a multi-variant Gaussian data set, albeit the sparse and inhomogeneous sampling. The corresponding *posterior* PDF is a multivariate Gaussian that is completely determined by the assumed PS and covariance matrix of errors. Under these conditions one can write the joint PDF of the model PS and the underlying velocity or density field.

The purpose of the present study is to calculate, from the joint PDF, the PS and 3D mass distribution, as well as the 3D peculiar velocity field, as derived from the newly completed ENEAR galaxy peculiar velocity catalog (da Costa *et al.* 2000a, Paper I). First, the PS model parameters are estimated by maximizing the likelihood function given the model (Zaroubi *et al.* 1997). An identical likelihood estimation of the power spectrum has been previously applied to the Mark III (Zaroubi *et al.* 1997) and the SFI (Freudling *et al.* 1999) data sets. In both cases the analysis yielded a high amplitude power spectrum. Although the results from those two catalogs are consistent with each other, they are marginally inconsistent with the power spectra measured from redshift catalogs (*e.g.*, da Costa *et al.* 1996; Sutherland *et al.* 1999), inferred from the analysis of the velocity

correlation function (*e.g.* Borgani *et al.* 2000a, 2000b), and from velocity-velocity comparisons (*e.g.*, Davis *et al.* 1996, da Costa *et al.* 1998). One of our goals is to use the same methodology employed before for the Mark III and SFI to the new ENEAR catalog to directly test the reproducibility of the results with an independent sample based on a different distance indicator but probing a comparable volume.

Second, the Wiener filter (WF) solution of the field is recovered by finding the most probable field given the PS and the data (Zaroubi *et al.* 1995, 1999). Constrained realizations (CR) are then used to sample the statistical scatter around the WF field (Hoffman and Ribak 1991). The mass density PS is used to calculate the smoothed Wiener filtered density and 3D velocity fields given the measured radial velocities (Zaroubi *et al.* 1995, 1999). The WF provides an optimal estimator of the underlying field in the sense of a minimum-variance solution given the data and an assumed *prior* model (Wiener 1949; Press *et al.* 1992). The *prior* defines the data auto-correlation and the data-field cross-correlation matrices. In the case where the data is drawn from a random Gaussian field, the WF estimator coincides with the conditional mean field and with the most probable configuration given the data (see Zaroubi *et al.* 1995). It should be noted that Kaiser & Stebbins (1991) were the first to propose a Bayesian solution to the problem of reconstruction from peculiar velocity data sets.

Finally, the recovered three-dimensional velocity field is used to compute the amplitude of the bulk flow and to decompose the velocity field in terms of a divergent and tidal components which enables one to separate the contribution to the measured peculiar velocity field from mass fluctuations within and outside the volume probed by the data (Hoffman *et al.* 2000).

The methods adopted in this study do not involve any explicit window function, weighting or smoothing the data. In addition, they automatically underweight noisy, unreliable data. However, a few simplifying assumptions are required: 1) peculiar velocities are drawn from a Gaussian random field; 2) peculiar velocities are related to the densities through linear theory; 3) errors in the $D_n - \sigma$ inferred distances constitute a Gaussian random field with two components, the first scales linearly with distance while the second models the nonlinear evolution of the velocities as a constant scatter. The need to assume a parametric functional form for the PS is also a limitation.

The outline of this paper is as follows. In § 2 we briefly describe the peculiar velocity data used in the present analysis. The PS analysis is carried out in § 3. The Wiener filtering is applied to the ENEAR data in § 4, where maps of the density field are presented and compared to those predicted from redshift surveys. Also shown in this section are the recovered three-dimensional velocity field and the results of its analysis. Our results are summarized and discussed in § 5.

2 THE DATA

In the present analysis, we use the ENEAR redshift-distance survey described in greater detail in Paper I of this series. Briefly, the ENEAR sample consists of roughly 1600 early-type galaxies brighter than $m_B = 14.5$ and with $cz \leq 7000$ km s⁻¹, for which $D_n - \sigma$ distances are avail-

able for 1359 galaxies. Of these 1145 were deemed suitable for peculiar velocity analysis according to well-defined criteria (Paper I; M. Alonso *et al.*, in preparation). To the magnitude-limited sample we added 285 fainter and/or with redshifts $> 7000 \text{ km s}^{-1}$, 129 within the same volume as the magnitude-limited sample. In total, the cluster sample consists of 569 galaxies in 28 clusters, which are used to derive the distance relation (M. Bernardi *et al.*, in preparation). Over 80% of the galaxies in the magnitude-limited sample and roughly 60% of the cluster galaxies have new spectroscopic and R-band photometric data obtained as part of this program. Furthermore, repeated observations of several galaxies in the sample (M. Alonso *et al.*, in preparation; G. Wegner *et al.* 2000) provide overlaps between observations conducted with different telescope/instrument configurations and with data available from other authors. These overlaps are used to tie all measurements into a common system, thereby ensuring the homogeneity of the entire dataset. In contrast to other samples new observations conducted by the same group are available over the entire sky. The comparison between the sample of galaxies with distances and the parent catalog also shows that the sampling across the sky is uniform.

Individual galaxy distances were estimated from a direct $D_n - \sigma$ template relation derived by combining all the available cluster data (M. Bernardi *et al.*, in preparation), corrected for incompleteness and associated diameter-bias (Lynden-Bell *et al.* 1988). From the observed scatter of the template relation the estimated fractional error in the inferred distance of a galaxy is $\Delta \sim 0.19$, nearly independent of the velocity dispersion.

Since early-type galaxies are found preferentially in high-density regions, galaxies have been assigned to groups/clusters using well-defined criteria imposed on their projected separation and velocity difference relative to the center of groups and clusters. These systems were identified using objective algorithms applied to the available magnitude-limited samples, comprising all morphological types, with complete redshift information probing the same volume. For membership assignment we used group catalogs published by Geller & Huchra (1983), Maia, da Costa & Latham (1988), Ramella, Pisani & Geller (1997) as well as unpublished results (M. Ramella *et al.*, in preparation) covering other regions of the sky. The characteristic size and velocity dispersion of these groups/clusters were used to establish the membership of the ENEAR early-types, as described in Paper I. We find isolated galaxies, groups with only one early-type, and groups with two or more early-types. Early-type galaxies in a group/cluster are replaced by a single object having: (1) the redshift given by the group's mean redshift, which is determined considering all morphologies; (2) the distance given by the error-weighted mean of the inferred distances, for groups with two or more early-types; and (3) the fractional distance error given by Δ/\sqrt{N} , where N is the number of early-types in the group. In some cases groups were identified with Abell/ACO clusters within the same volume as the ENEAR sample and fainter cluster galaxies were added, as described in Paper I. In the analysis below we compute the dipole component of the velocity field out to 6000 km s^{-1} as probed by all objects, and by splitting the sample into two independent sub-samples consisting of field galaxies and groups/clusters. The latter is done to eval-

uate directly from data the amplitude of possible sampling errors.

The inferred distances are corrected for the homogeneous and inhomogeneous Malmquist bias (IMB). The latter was estimated using the PCSz density field (Branchini *et al.* 1999), corrected for the effects of peculiar velocities, in the expressions given by Willick *et al.* (1997). In this calculation we also include the correction for the redshift limit of the sample. A complete account of the sample used and the corrections applied will be presented in a subsequent paper of this series (M. Alonso *et al.*, in preparation).

3 POWER SPECTRUM

The calculation of the matter PS from the peculiar velocity data by means of likelihood analysis requires a relation between the velocity correlation function and the power spectrum. Define the two-point velocity correlation (3×3) tensor by the average over all pairs of points \mathbf{r}_i and \mathbf{r}_j that are separated by $\mathbf{r} = \mathbf{r}_j - \mathbf{r}_i$,

$$\Psi_{\mu\nu}(\mathbf{r}) \equiv \langle v_\mu(\mathbf{r}_i)v_\nu(\mathbf{r}_j) \rangle, \quad (1)$$

where $v_\mu(\mathbf{r}_i)$ is the μ component of the peculiar velocity at \mathbf{r}_i . In linear theory, it can be expressed in terms of two scalar functions of $r = |\mathbf{r}|$ (Górski 1988), computed from the parallel and perpendicular components of the peculiar velocity, relative to the separation vector \mathbf{r} ,

$$\Psi_{\mu\nu}(\mathbf{r}) = \Psi_\perp(r)\delta_{\mu\nu} + [\Psi_\parallel(r) - \Psi_\perp(r)]\hat{\mathbf{r}}_\mu\hat{\mathbf{r}}_\nu. \quad (2)$$

The spectral representation of these radial correlation functions is

$$\Psi_{\perp,\parallel}(r) = \frac{H_0^2 f^2(\Omega)}{2\pi^2} \int_0^\infty P(k) K_{\perp,\parallel}(kr) dk, \quad (3)$$

where $K_\perp(x) = j_1(x)/x$ and $K_\parallel(x) = j_0 - 2j_1(x)/x$, with $j_l(x)$ the spherical Bessel function of order l . The cosmological Ω dependence enters as usual in linear theory via $f(\Omega) \approx \Omega^{0.6}$, and H_0 is the Hubble constant. A parametric functional form of $P(k)$ thus translates to a parametric form of $\Psi_{\mu\nu}$. Note that the quantity that can be derived from peculiar-velocity data via the linear approximation is $f^2(\Omega)P(k)$, where P is the mass density PS.

Let \mathbf{m} be the vector of model parameters and \mathbf{d} the vector of N data points. Then Bayes' theorem states that the *posterior* probability density of a model given the data is

$$\mathcal{P}(\mathbf{m}|\mathbf{d}) = \frac{\mathcal{P}(\mathbf{m})\mathcal{P}(\mathbf{d}|\mathbf{m})}{\mathcal{P}(\mathbf{d})}. \quad (4)$$

The denominator is merely a normalization constant. The probability density of the model parameters, $\mathcal{P}(\mathbf{m})$, is unknown, and in the absence of any other information we assume it is uniform within a certain range. The conditional probability of the data given the model, $\mathcal{P}(\mathbf{d}|\mathbf{m})$, is the likelihood function, $\mathcal{L}(\mathbf{d}|\mathbf{m})$. The objective in this approach, which is to find the set of parameters that maximizes the probability of the model given the data, is thus equivalent to maximizing the likelihood of the data given the model (cf. Zaroubi *et al.* 1997; Jaffe & Kaiser 1994). The Bayesian analysis measures the relative likelihood of different models. An absolute frequentist's measure of goodness of fit is

provided by the χ^2 per degree of freedom (hereafter, *d.o.f.*), which we use as a check of the best parameters obtained by the likelihood analysis.

Assuming that the velocities are a Gaussian random field, the two-point velocity correlation tensor Ψ fully characterizes the statistics of the velocity field. Define the radial-velocity correlation ($N \times N$) matrix U_{ij} by

$$U_{ij} = \hat{\mathbf{r}}_i \dagger \Psi \hat{\mathbf{r}}_j = \Psi_{\perp}(r) \sin\theta_i \sin\theta_j + \Psi_{\parallel}(r) \cos\theta_i \cos\theta_j, \quad (5)$$

where i and j refer to the data points, $r = |\mathbf{r}| = |\mathbf{r}_j - \mathbf{r}_i|$ and the angles are defined by $\theta_i = \hat{\mathbf{r}}_i \cdot \hat{\mathbf{r}}$ (Górski 1988; Groth, Juszkiewicz & Ostriker 1989). Let the inferred radial peculiar velocity at \mathbf{r}_i be u_i^o , with the corresponding error ϵ_i also assumed to be a Gaussian random variable. The observed correlation matrix is then $\tilde{U}_{ij} = U_{ij} + \epsilon_i^2 \delta_{ij}$, and the likelihood of the N data points is

$$\mathcal{L} = [(2\pi)^N \det(\tilde{U}_{ij})]^{-1/2} \exp\left(-\frac{1}{2} \sum_{i,j} u_i^o \tilde{U}_{ij}^{-1} u_j^o\right). \quad (6)$$

Given that the correlation matrix, \tilde{U}_{ij} , is symmetric and positive definite, we can use the Cholesky decomposition method (Press *et al.* 1992) for computing the likelihood function (Eq. (6)). The significant contribution of the errors to the diagonal terms makes the matrix especially well-conditioned for decomposition.

The errors are assumed to have two contributions, the first is the usual $D_n - \sigma$ distance proportional errors (about 19% per galaxy for ENEAR). The second is a constant error that accounts for the non-linear velocities of galaxies in the high density environment in which early-type galaxies reside. This term represents our poor understanding of the complex correlations introduced by non-linear evolution. For each power spectrum model, we have performed the likelihood analysis assuming this constant value to be either null or 250 km s^{-1} but, as shown below, the difference in the results are only marginal and do not affect our general conclusions.

3.1 COBE-Normalized CDM Models

We first restrict our attention to the generalized family of CDM cosmological models, allowing variations in the cosmological parameters Ω , Λ and h . Furthermore, four-year COBE normalization is imposed as an additional external constraint. The general form of the PS for these models is

$$P(k) = A_{\text{COBE}}(n, \Omega, \Lambda) T^2(\Omega, \Omega_B, h; k) k^n, \quad (7)$$

where the CDM transfer function proposed by Sugiyama (1995) is adopted,

$$T(k) = \frac{\ln(1 + 2.3q)}{2.34q} [1 + 3.89q + (16.1q)^2 + (5.46q)^3 + (6.71q)^4]^{-1/4} \quad (8)$$

$$q = k \left[\Omega h \exp(-\Omega_b - h_{50}^{1/2} \Omega_b / \Omega) (h \text{ Mpc}^{-1}) \right]^{-1}. \quad (9)$$

The parameters Ω and h are varied such that they span the range of currently popular CDM models, including Λ CDM ($\Omega + \Lambda = 1$, $\Omega \leq 1$) and OCDM ($\Lambda = 0$, $\Omega \leq 1$). In all cases, the baryonic density is assumed to be $\Omega_b = 0.019h^{-2}$, which

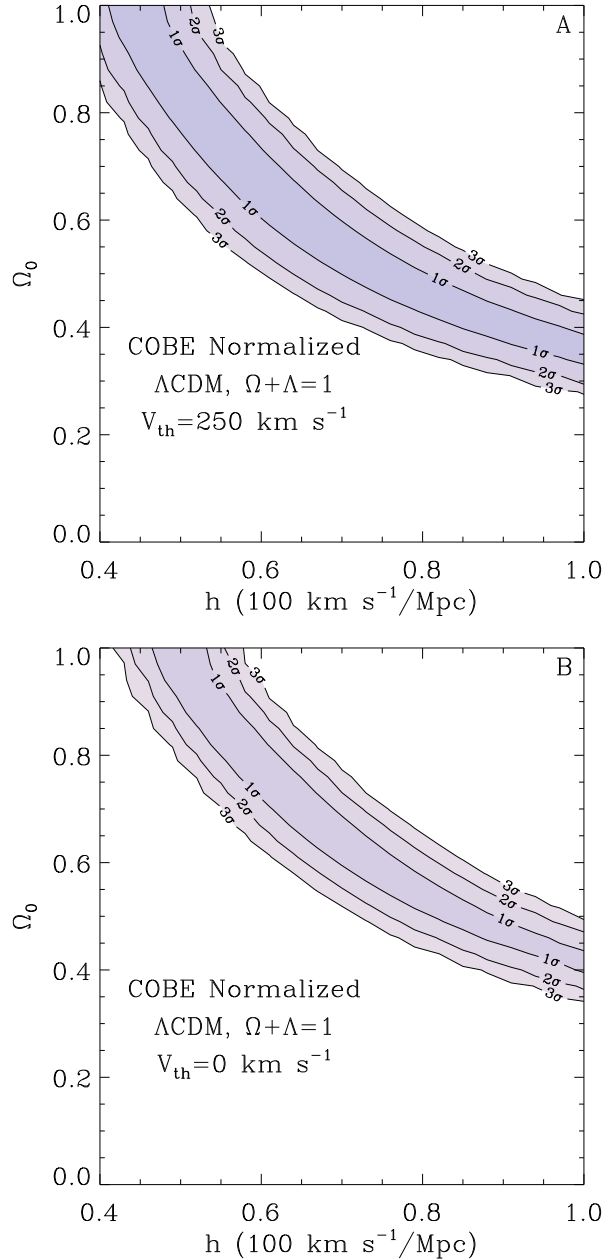


Figure 1. Contour map of \ln -likelihood in the $h - \Omega$ plane for Λ CDM models with 250 km s^{-1} thermal error component (upper panel) and with zero thermal error (lower panel). The contours denote the most likely values within 1, 2 and 3σ *c.l.*

is the value currently favored by primordial nucleosynthesis analysis (*e.g.*, Burles & Tytler 1998). We limit our inquiry to models without tilt, namely to models with $n = 1$. For each model, the normalization of the PS is fixed by the COBE 4-year data (Bennet *et al.* 1996); for more details see Zaroubi *et al.* (1997 and references therein).

Figure 1a shows the likelihood contour map in the $\Omega - h$ plane, for the Λ CDM family of models with $n = 1$ (normalization by Sugiyama 1995), the error matrix is assumed here to have an additional diagonal random contribution of 250 km s^{-1} that accounts for the nonlinear evolution of the galaxies. The most probable parameters in this case (in the range $\Omega \leq 1$) are $\Omega = 1$ and $h = 0.5$. The elongated contours clearly indicate that neither Ω nor h are independently well

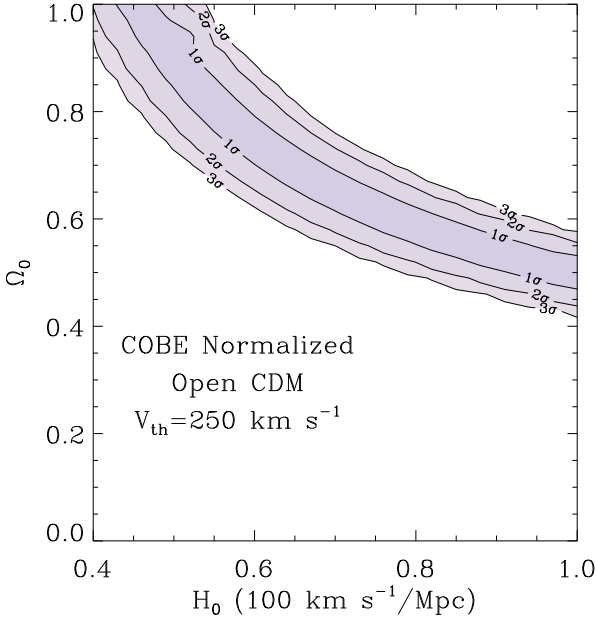


Figure 2. Same as in Figure 1a but for OCDM models.

constrained. It is rather a degenerate combination of the two parameters, approximately Ωh^x with $x \sim 1$ (*i.e.* a combination close to the Γ parameter) that is being determined tightly by the elongated ridge of high likelihood.

Figure 1b shows the likelihood results for the same Λ CDM model shown in Fig. 1a but with no random contribution to the error matrix. The contours in Fig. 1b show very little changes relative to those shown in panel (a), notably they get tighter and the best values of Ω for a given Hubble constant are somewhat higher. The addition of a reasonable random component to the error matrix does not alter the results in any significant way for any of the PS models considered in this study. For the rest of the PS models we show the calculation with the addition of a constant error of 250 km s^{-1} .

Figure 2 shows the similar likelihood map for OCDM with $n = 1$. The most probable values here are $\Omega = 0.53$ and $h = 1$. The values of Ω and h are not independently constrained here as well.

We can thus quote stringent constraints on the conditional best value of Ω given h for the COBE normalized CDM models shown in Figs. 1a and 2: $\Omega \approx (0.377 \pm 0.08)h^{-1.3}$ for Λ CDM, and $\Omega \approx (0.517 \pm 0.083)h^{-0.88}$ for OCDM.

3.2 The Γ Model

To recover the PS from the velocity data independent of the COBE normalization, we use as a parametric prior the so-called Γ model (*e.g.*, Efstathiou, Bond and White 1992),

$$P(k) = AkT^2(k),$$

$$T(k) = \left(1 + [ak/\Gamma + (bk/\Gamma)^{3/2} + (ck/\Gamma)^2]^\nu\right)^{-1/\nu} \quad (10)$$

with $a = 6.4 h^{-1} \text{Mpc}$, $b = 3.0 h^{-1} \text{Mpc}$, $c = 1.7 h^{-1} \text{Mpc}$ and $\nu = 1.13$. The free parameters to be determined by the likelihood analysis are the normalization factor $\eta_8 \equiv \sigma_8 \Omega^{0.6}$

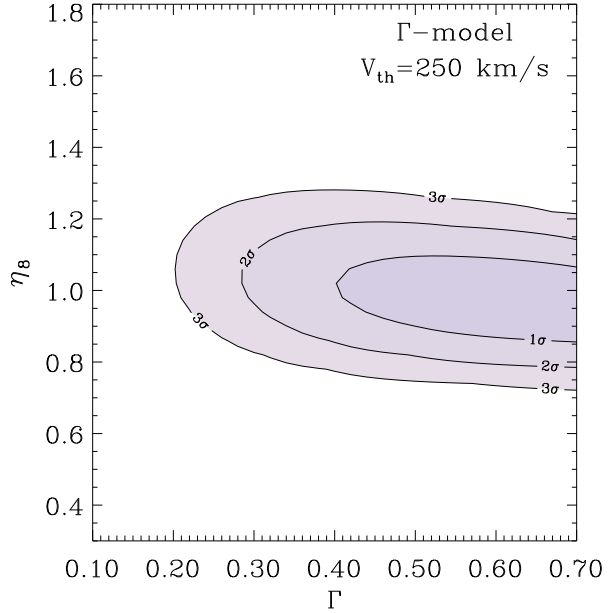


Figure 3. Contour map of \ln -likelihood for the Γ model in the $\Gamma - \eta_8$ plane. The contours denote the 1, 2 and 3σ

c.l.

and the Γ parameter. In the context of the CDM cosmological model, Γ has a specific cosmological interpretation, $\Gamma = \Omega h$. Here, however, Eq. (10) serves as a generic function with logarithmic slopes $n = 1$ and -3 on large and small scales respectively, and with a turnover at some intermediate wavenumber that is determined by the single shape parameter Γ .

Figure 3 shows the contour map of $\ln\mathcal{L}$ in the $\Gamma - \eta_8$ plane. Although the likelihood analysis poses strong constraint on the allowed values of η_8 ($= 1.0^{+0.3}_{-0.28}$ with 3σ *c.l.*), it only weakly constrains the value of Γ (≥ 0.18 with 3σ *c.l.*), and $\Gamma = 0.25$ is excluded with 2σ *c.l.*

3.3 Results and Comparison between the Various Models

The best fit models for each CDM family have a comparable likelihood, with the most likely model is the OCDM model with $\Omega = 0.53$ and $h = 1$. All best fit models agree within $\approx 20\%$ for $k > 0.1 h \text{Mpc}^{-1}$. The amplitude of the PS at $k = 0.1 h \text{Mpc}^{-1}$ for all models lies within $P(k)\Omega^{1.2} = (6.5 \pm 3) \times 10^3 (h^{-1} \text{Mpc})^3$ and the values of η_8 are within the range $1.1^{+0.2}_{-0.35}$.

Figure 4 shows the power spectrum of the most-likely COBE-normalized model and the 3σ errors about it. It also shows the PS corresponding to most likely models of Λ CDM and Γ models. Within the errors, the most likely PS for each CDM family are very consistent, especially at intermediate scales ($30 - 50 h^{-1} \text{Mpc}$), where the data information content provide the strongest constraint. Also shown in Fig. 4 are the best-fit PS, obtained from a similar likelihood analysis, for the Mark III and SFI data sets. As can be seen the most likely PS for the three catalogs are in good agreement. This result shows that the high amplitude PS found from peculiar velocity data is unlikely to be due to possible non-uniformities of these catalogs or to the type of galaxies

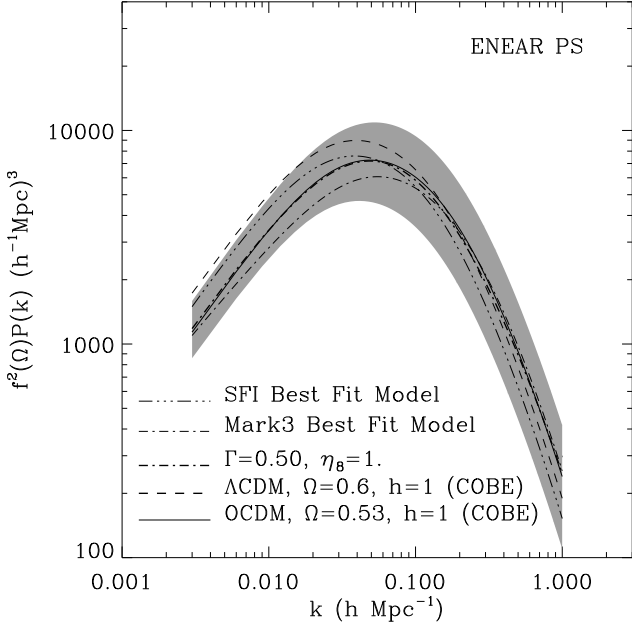


Figure 4. The PS of the most probable COBE-normalized OCDM (solid-bold) and Λ CDM (dashed-bold) models and of the Γ -model (dotted-dashed-bold). shown also the most probable models as estimated from Mark III (dotted-dashed) and SFI (triple-dotted-dashed) data sets. The shaded region around the PS marks the $3\text{-}\sigma$ *c.l.* note that the dynamical range of the data is confined to $0.05 \lesssim k \lesssim 0.3$.

used. In fact, while Mark III and SFI relied predominantly on TF distances to spirals, ENEAR relies on $D_n - \sigma$ distances to early-type galaxies. On the other hand, the reason for the discrepancy in the cosmological constraints between the maximum likelihood method and other methods (da Costa *et al.* 1998; Strauss & Willick 1998; Borgani *et al.* 2000a, 2000b) remains unresolved. The former yields a systematically higher amplitude PS, as reflected by the high values of η_8 , which is also in disagreement with the constraints derived from other analysis of LSS data. Possible explanations are given in § 5.

In all the COBE-normalized PS models considered the $\chi^2/d.o.f.$ of the best fit models is of the order of 0.93. This value deviates by about 2σ from the $\chi^2/d.o.f.$ desired value of unity. This, however, does not pose any serious problem since many of the models within the likelihood most likely contours have a $\chi^2/d.o.f. \simeq 1$. The $\chi^2/d.o.f.$ for the Γ -model is 0.99.

4 WIENER FILTER & CONSTRAINED REALIZATIONS

4.1 The Method

Having determined the power spectrum, all the ingredient needed to Wiener reconstruct the density and velocity fields are ready. Details on the general application of the WF/CR method to the reconstruction of large-scale structure are described in Zaroubi *et al.* (1995), where the theoretical foundation is discussed in relation with other methods of estimation, such as Maximum Entropy. The specific application of the WF/CR method to peculiar velocity data sets has been

presented in Zaroubi *et al.* (1999). Here we provide only a brief description of the WF/CR method, for more details the reader is referred to the original references given above.

We assume that the peculiar velocity field $\mathbf{v}(\mathbf{r})$ and the density fluctuation field $\delta(\mathbf{r})$ are related via linear gravitational-instability theory. Under the assumption of a specific theoretical prior for the power spectrum $P(k)$ of the underlying density field, one can write the WF minimum-variance estimator of the fields as

$$\mathbf{v}^{\text{WF}}(\mathbf{r}) = \left\langle \mathbf{v}(\mathbf{r}) u_i^o \right\rangle \left\langle u_i^o u_j^o \right\rangle^{-1} u_j^o \quad (11)$$

and

$$\delta^{\text{WF}}(\mathbf{r}) = \left\langle \delta(\mathbf{r}) u_i^o \right\rangle \left\langle u_i^o u_j^o \right\rangle^{-1} u_j^o. \quad (12)$$

A well known problem of the WF is that it attenuates the estimator to zero in regions where the noise dominates. The reconstructed mean field is thus statistically inhomogeneous. In order to recover statistical homogeneity we produce constrained realizations (CR), in which random realizations of the residual from the mean are generated such that they are statistically consistent both with the data and the *prior* model (Hoffman and Ribak 1991; see also Bertschinger 1987). In regions dominated by good quality data, the CRs are dominated by the data, while in the limit of no data the realizations are practically unconstrained.

The CR method is based on creating random realizations, $\tilde{\delta}(\mathbf{r})$ and $\tilde{\mathbf{v}}(\mathbf{r})$, of the underlying fields that obey the assumed PS and linear theory, and a proper set of random errors $\tilde{\epsilon}_i$. The velocity random realization is then “observed” like the actual data to yield a mock velocity dataset \tilde{u}_i^o . Constrained realizations of the dynamical fields are then obtained by

$$\mathbf{v}^{\text{CR}}(\mathbf{r}) = \tilde{\mathbf{v}}(\mathbf{r}) + \left\langle \mathbf{v}(\mathbf{r}) u_i^o \right\rangle \left\langle u_i^o u_j^o \right\rangle^{-1} (u_j^o - \tilde{u}_j^o) \quad (13)$$

and

$$\delta^{\text{CR}}(\mathbf{r}) = \tilde{\delta}(\mathbf{r}) + \left\langle \delta(\mathbf{r}) u_i^o \right\rangle \left\langle u_i^o u_j^o \right\rangle^{-1} (u_j^o - \tilde{u}_j^o). \quad (14)$$

The two types of covariance matrices in the above equations are computed within the framework of linear theory as follows. The covariance matrix of the data $\left\langle u_i^o u_j^o \right\rangle$ is the same matrix \tilde{U}_{ij} that appears in eq. 6.

The cross-correlation matrix of the data and the underlying field enters the above equations as, *e.g.*,

$$\left\langle \delta(\mathbf{r}) u_j^o \right\rangle = \left\langle \delta(\mathbf{r}) \mathbf{v}(\mathbf{r}_j) \right\rangle \cdot \hat{\mathbf{r}}_j. \quad (15)$$

The two-point cross-correlation vector between the density and velocity fields is related to the PS via

$$\left\langle \delta(\mathbf{x}) \mathbf{v}(\mathbf{x} + \mathbf{r}) \right\rangle = -\frac{H_0 f(\Omega_0)}{2\pi^2} \hat{\mathbf{r}} \int_0^\infty k P(k) j_1(kr) dk. \quad (16)$$

The assumption that linear theory is valid on all scales enables us to choose the resolution as well, and in particular to use different smoothing radii for the data and for the recovered fields. In our case no smoothing were applied to the radial velocity data while we choose to reconstruct the density field with a finite Gaussian smoothing of radius R . This alters the density-velocity correlation function by inserting

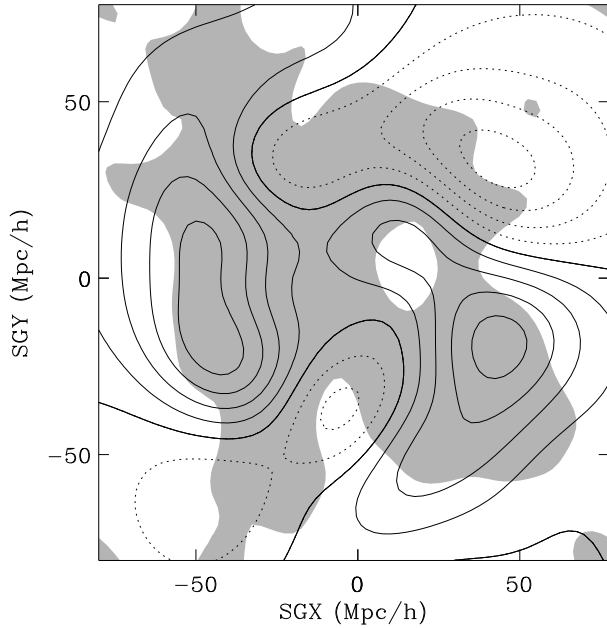


Figure 5. Reconstruction from the ENEAR catalog. Left panel: The density field map in the Supergalactic plane, with G12 smoothing. Density contour spacing is 0.1, positive contours are solid, negative contours are dashed and $\delta = 0$ is denoted by heavy-solid line. The shading indicates regions where the error is less than 0.3.

the multiplicative term $\exp[-k^2 R^2/2]$ into the integrand of eq. (16).

A theoretical estimate of the signal-to-noise ratio (S/N) at every point in space is given by a simple expression (see Zaroubi *et al.* 1999) but it requires the calculation and inversion of very large matrices. Therefore, in this study we estimate the point to point error by conducting a large number of CRs. In the case of random Gaussian fields, the ensemble of CRs defined in eq. (13) and eq. (14) samples the distribution of uncertainties in the mean Wiener density and velocity fields (Hoffman & Ribak 1991).

It is worth noting that the WF represents a general minimum-variance solution under the sole assumption that the field is a random field with a known power spectrum. No assumption has to be made here regarding higher order correlations (or the full joint probability distribution functions) of the underlying field. On the other hand, the CRs are derived under the explicit assumption of a full Gaussian random field.

4.2 Maps of Density and Velocity Fields

Figure 5 shows the map of the density field along the Supergalactic plane obtained from the ENEAR data using a Gaussian smoothing radius of 1200 km s^{-1} (hereafter G12). The shaded area corresponds to the region where the error, as estimated from performing 10 CRs, in density is less than 0.3. The main features of our local universe are easily identified in the WF map, including the Great Attractor (GA) on the left and the Perseus-Pisces supercluster (PP) in the lower right. There is also a hint of the Coma cluster, which lies

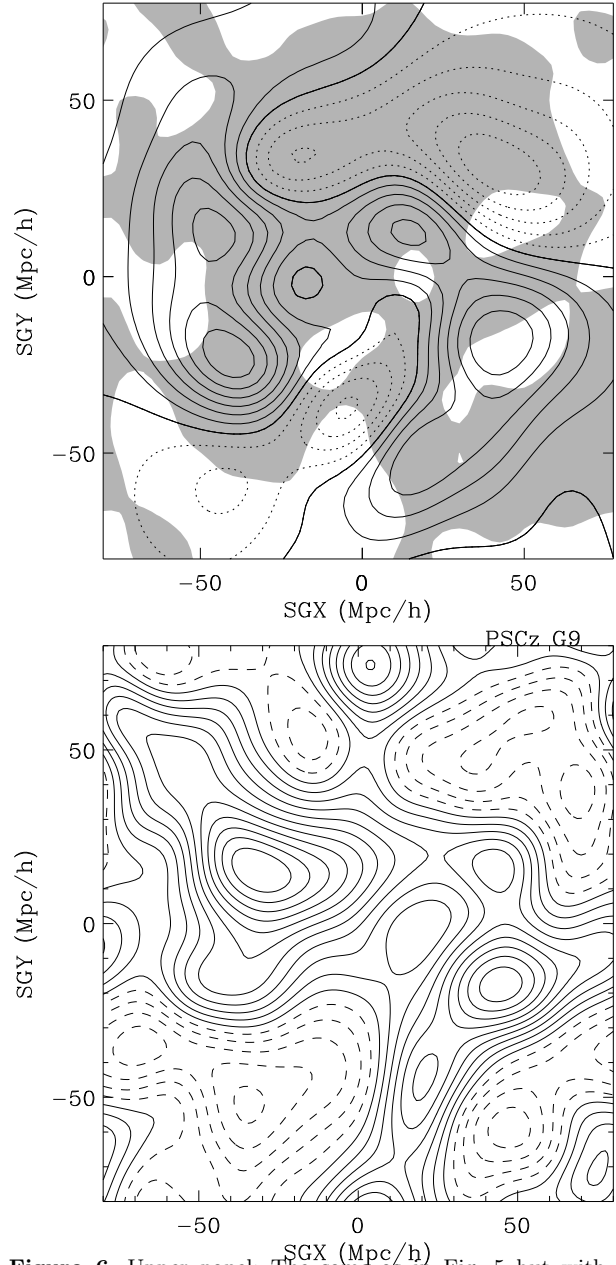


Figure 6. Upper panel: The same as in Fig. 5 but with G9 smoothing. The shaded area indicates regions with error smaller than 0.45. Lower panel: The G9 smoothing density reconstruction from the PSCz redshift catalog (Branchini *et al.* 1999)

just outside the sample, in the upper part on the map. Even though different in details, the gross features of the density field are remarkably similar to those obtained by Zaroubi, Hoffman & Dekel (1999) from the application of the same formalism to the Mark III catalog. This is an outstanding result considering the different ways the two catalogs were constructed and the peculiar velocities measured.

Fig. 6 compares a higher resolution map of the density field recovered from the ENEAR data (left panel) to the density field reconstructed from the PSCz redshift catalog (right panel; Branchini *et al.* 1999). Both maps are along the Supergalactic plane and were reconstructed using a 900 km s^{-1} smoothing radius. The shaded area in the left panel indicates regions where the error is less than 0.45. Even though differ-

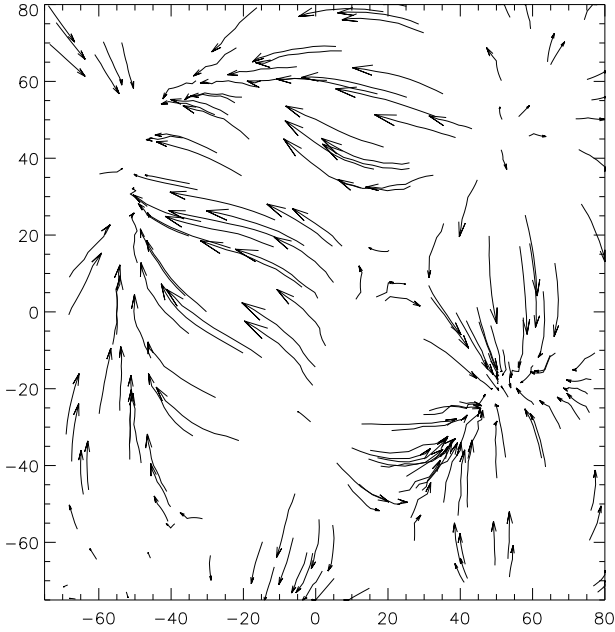


Figure 7. The G12 reconstructed velocity field in the Supergalactic plane is displayed as flow lines that start at random points, continue tangent to the local velocity field, and are of length proportional to the magnitude of the velocity at the starting point.

ent in detail the similarities between the density fields are striking lending further credence to the reality of the structures observed in the mass distribution. Note that with the higher resolution some structures become resolved. One can clearly see the Local supercluster at the center of the map and that both the GA and PP may consist of different substructures.

The velocity field along the Supergalactic plane is presented in Fig. 7, showing the existence of two convergence regions which roughly coincide with the locations of the GA and PP.

4.3 Bulk Velocity

The velocity field has been fitted using a monopole, dipole (*i.e.* bulk flow) and quadrupole (*i.e.* shear) expansion within spheres of radii ranging from 1000 to 6000 km s^{-1} . The three Cartesian components of the bulk velocity (in Supergalactic coordinates) and its absolute value (V_B) are shown in Fig. 8 as a function of the depth over which the fit has been done. The plots present the bulk velocity of the WF field and of an ensemble of 10 CRs. The plot of the absolute value of the bulk velocity contains also the mean and standard deviation calculated over the ensemble of the CRs. Note that the mean V_B of the CRs is higher than its WF value. This result is expected as the WF attenuates the velocity field with the depth, as the observational errors become more dominant.

The amplitude of the bulk flow measured from the reconstructed three-dimensional velocity field ranges from $V_B = 300 \pm 70 \text{ km s}^{-1}$ for a sphere of $R = 20 h^{-1} \text{ Mpc}$ to $160 \pm 60 \text{ km s}^{-1}$ for $R = 60 h^{-1} \text{ Mpc}$. This value is in good agreement with that obtained from a direct fit to the ra-

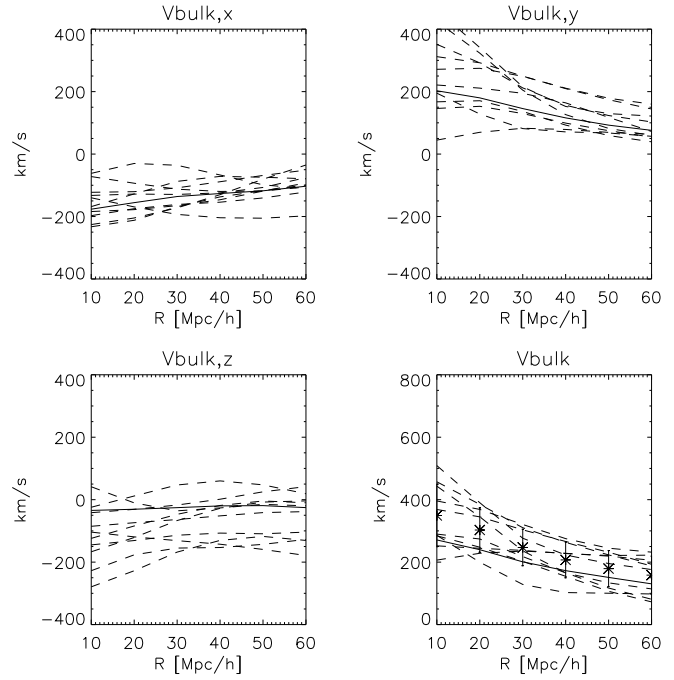


Figure 8. The bulk velocity fit of the reconstructed velocity field as a function of depth: The solid line corresponds to the WF field and the dashed lines correspond to an ensemble of 10 CRs. The four panels show the (Super Galactic) x,y and z components and the amplitude of the bulk velocity. The bottom-right panel presents also the mean amplitude taken over the CRs and the error-bars are the standard deviation around it. Note that this mean value is expected to be larger than the amplitude of the WF bulk velocity.

dial peculiar velocities (da Costa *et al.* 2000b). This result disagrees with the bulk flow determination from the Mark III survey where the amplitude is roughly twice that of EN-EAR with a comparable scatter (Zaroubi *et al.* 1999) but comparable to that measured from the SFI sample.

4.4 Large Scale Tidal field

An alternative way of describing the velocity field is to decompose it into two components, one which is induced by the local mass distribution and a tidal component due to mass fluctuations external to the volume considered. Here we follow the procedure suggested by Hoffman (1998a,b) and more recently by Hoffman *et al.* (2000). The key idea is to solve for the particular solution of the Poisson equation with respect to the WF density field within a given region and zero padding outside. This yields the velocity field induced locally, hereafter the divergent field. The tidal field is then obtained by subtracting the divergent field from the full velocity field. Fig. 9 shows the results of this decomposition applied to the ENEAR survey, where the local volume is a sphere of $80 h^{-1} \text{ Mpc}$ centered on the Local Group. The plots show the full velocity field (upper left panel), the divergent (upper right panel) and the tidal (lower left panel) components. To further understand the nature of the tidal field its bulk velocity component has been subtracted and the residual is shown in the lower right panel. This residual is clearly dominated by a quadrupole component. In princi-

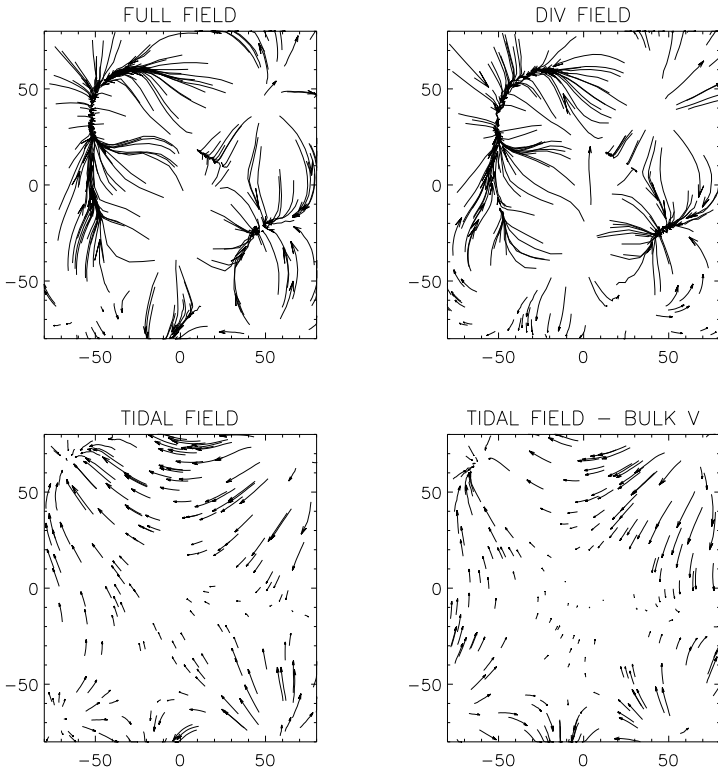


Figure 9. Tidal field decomposition of the G5 reconstructed velocity field in the Supergalactic plane is displayed as flow lines. The top-left panel shows to the full velocity field.

ple, the analysis of this residual field can shed light on the exterior mass distribution.

For the ENEAR catalog we find that the local dynamics is hardly affected by structure on scales larger than its depth. For this sample not only the bulk velocity at large radii is small but so is the rms value of the tidal field estimated to be of the order of 60 km s^{-1} . This is in marked contrast to the results obtained from the analysis of the Mark III survey which yields a much stronger tidal field, pointing (in the sense of its quadrupole moment) towards the Shapley concentration. For Mark III the tidal field contributes roughly third of the total bulk velocity ($\sim 200 \text{ km/s}$).

5 CONCLUSION

In the first part of this paper the maximum-likelihood method (Zaroubi *et al.* 1997) has been used to measure the mass-density power spectrum from the newly completed ENEAR early-type redshift-distance survey. The method assumes that the galaxy peculiar velocities satisfy Gaussian random statistics and that they are linearly related to the mass-density field. The initial fluctuation power spectrum is assumed to be CDM-like, with or without COBE normalizations. In addition the measured peculiar velocities error are assumed to be proportional to the distance with some thermal component to account for the nonlinear evolution of high-density environment in which the early-type galaxies reside.

General results that are valid for all the models used in the analysis, and are independent of the detailed parameter-

ization and normalization used in each model, can be summarized as follows. The amplitude of the power spectrum at $k = 0.1 h \text{ Mpc}^{-1}$ is $P(k)\Omega^{1.2} = (6.5 \pm 3) \times 10^3 (h \text{ Mpc}^{-1})^3$ yielding $\eta_8 = 1.1^{+0.2}_{-0.35}$. For the family of COBE-normalized CDM models the following range of parameters was considered: $\Omega \leq 1$; $0.4 < h < 1$; and $n = 1$. Within this range we have obtained a constraint on a combination of the parameters Ω and h which can be approximated by $\Omega \approx (0.38 \pm 0.08)h^{-1.3}$ for Λ CDM, and $\Omega \approx (0.52 \pm 0.083)h^{-0.88}$ for OCDM. For $h = 0.65$, Λ CDM yields $\Omega = 0.5 - 0.8$. Similar constraints are obtained from the analysis of the generic Γ -models, independent of the COBE normalization. We find that the power spectrum amplitude and shape parameter are constrained to be $\eta_8 = 1.0^{+0.3}_{-0.28}$ and $\Gamma \geq 0.18$, with larger values of Γ (> 0.4) being more probable. We point out that these constraints are consistent with the results obtained from a similar analysis of the Mark III and the SFI peculiar velocity catalogs. This agreement is encouraging since it shows that the results are robust and independent of the sample used.

Examination of the $\chi^2/d.o.f.$ for the most likely COBE-normalized models shows that their values are of the order of 0.93. These values are about 2σ away from the preferred value of 1. However, this should not be too alarming as many of the models within the errors have $\chi^2/d.o.f. \sim 1$. The $\chi^2/d.o.f.$ for the best-fit Γ -model is 0.99.

As pointed out by previous papers that have analyzed the PS derived from peculiar velocity data (Zaroubi *et al.* 1997, Freudling *et al.* 1999), the constraints on η_8 and Γ are considerably higher than those obtained from other types of analyzes including peculiar velocity data (Borgani *et al.* 1997, 2000), cluster abundances, and the galaxy power-spectrum (Efstathiou *et al.* 1992; Sutherland *et al.* 1999). They are also not consistent with those obtained by combining the results from high redshift supernovae type Ia (Perlmutter *et al.* 1999) and the CMB data (Efstathiou *et al.* 1999) which yields values of $\Omega \approx 0.25 \pm 0.15$ and $\Lambda \approx 0.65 \pm 0.2$. Furthermore, assuming a linear galaxy-mass relation the value of η_8 obtained from the present analysis would imply $\beta = 1.0$ or a $\beta_I \sim 1.4$ (*e.g.* Willmer, da Costa & Pellegrini 1999; Sutherland *et al.* 1999), where the subscript refers to *IRAS* galaxies, at least a factor of 2 larger than those derived from a velocity-velocity comparison of the *IRAS* 1.2 Jy gravity field and the Mark III (Davis *et al.* 1996), SFI (da Costa *et al.* 1998) and ENEAR (Nusser *et al.* 2000) all leading to $\beta_I \sim 0.5$. These values are also consistent with those derived from small-scale velocities (Fisher *et al.* 1995).

There are many possible explanations for the above discrepancies. One possibility is that all other analyses have somehow conspired to produce consistent results but yet incorrect interpretation. Even though at first glance this seems unlikely, the recent results from the CMB balloon experiments Boomerang (Bernardis *et al.* 2000; Lange *et al.* 2000) and MAXIMA (Hanany *et al.* 2000; Balbi *et al.* 2000) have shown that the height of the second peak in the CMB angular power-spectrum is consistent with higher values of Ω . From their most likely models these authors derive $\Omega = 0.4 - 0.8$.

It is important to point out that the method is very sensitive to the assumed error model which can add or suppress power. It also implicitly gives a high weight to nearby

galaxies, likely to be slow rotators or low velocity dispersion systems, for which the measurements and the distance relations are the least reliable. However, tests have shown that these effects are not very important for the present data set. Another potential problem arises due to the rapid decrease of the weight with distance, the effective volume of the currently available catalogs is small and the shape of the power spectrum is poorly constrained, as illustrated by the case of the Γ -model. All these factors may impact on the reliability of the constraints obtained from the PS analysis.

Finally, one or more of the theoretical model ingredients could be inaccurate, *e.g.*, power spectrum assumed shapes, Gaussianity of the distribution; or even some inherent bias in the method itself that has eluded the extensive numerical tests carried out with the data and mock samples (*e.g.* Freduling *et al.* 1999). In fact, through an eigenmode expansion of the Mark III and SFI galaxy catalogs, Hoffman and Zaroubi (2000) have conducted a mode-by-mode goodness-of-fit analysis. They found that when the surveys are analyzed with their corresponding CDM most likely models, there is a systematic inconsistency between the data and the ‘best-fit’ models suggesting either a generic problem in the peculiar velocity data sets or the inadequacy of the theoretical or error models. Unfortunately, however, the analysis has not been able to point to the exact source of inconsistency.

Finally, in this study we have also performed, given the most probable power spectrum, a Wiener reconstruction of the density and velocity fields. The maps shown here have 1200 km s^{-1} and 900 km s^{-1} Gaussian resolution and they are limited to the Supergalactic plane. The main features shown are similar to the features in the *IRAS* reconstruction, corrected for peculiar velocities. The constrained realizations allow us to estimate the point-by-point uncertainties in the recovered maps. In terms of their recovered density fields ENEAR, SFI and Mark III mostly agree. However, they do differ in the velocity fields. ENEAR shows no significant tidal component which contributes about half of the Mark III local bulk velocity. This tidal field accounts for the very different bulk velocities obtained from ENEAR and Mark III, with SFI situated in between these surveys. The results suggest that volumes of $60 - 80 h^{-1} \text{ Mpc}$ are essentially at rest relative to the CMB and that the Local Group motion is primarily due to mass fluctuations within the volume sampled by the existing catalogs of peculiar velocity data.

6 ACKNOWLEDGMENTS

We thank Enzo Branchini for providing the PSCz density field. We acknowledge Avishai Dekel, Enzo Branchini, Tony Banday, Ravi Sheth, Simon White and Idit Zehavi for stimulating discussions. SZ gratefully acknowledge the hospitality of Kapteyn Astronomical Institute – Groningen. The authors would like to thank M. Maia, C. Rit e and O. Chaves for their contribution over the years. MB thanks the Sternwarte M unchen, the Technische Universit at M unchen, ESO Studentship program, and MPA Garching for their financial support during different phases of this research. MVA is partially supported by CONICET, SecyT and the Antorchas-Andes- Vitae cooperation. GW is grateful to the Alexander

von Humboldt-Stiftung for making possible a year’s stay at the Ruhr-Universit at in Bochum, and to ESO for support for visits to Garching which greatly aided this project. Financial support for this work has been given through, Israel Science Foundation grant 103/98 (YH), FAPERJ (CNAW, MAGM, PSSP), CNPq grants 201036/90.8, 301364/86-9 (CNAW), 301366/86-1 (MAGM); NSF AST 9529098 (CNAW); ESO Visitor grant (CNAW). PSP and MAGM thank CLAF for financial support and CNPq fellowships. The results of this paper are based on observations at Complejo Astronomico El Leoncito (CASLEO), operated under agreement between the Consejo Nacional de Investigaciones Cient ficas de la Rep blica Argentina and the National Universities of La Plata, C rdoba and San Juan; Cerro Tololo Interamerican Observatory (CTIO), operated by the National Optical Astronomical Observatories, under AURA; European Southern Observatory (ESO), partially under the ESO-ON agreement; Fred Lawrence Whipple Observatory (FLWO); Observat rio do Pico dos Dias, operated by the Laborat rio Nacional de Astrof sica (LNA); and the MDM Observatory at Kitt Peak

REFERENCES

- Balbi A., Ade P., Bock J., Borrill J., Boscaleri A., de Bernardis P., Ferreira P. G., Hanany S., Hristov V.V., Jaffe A.H., Lee A. T., Oh S., Pascale Y., Rabii B., Richards P.L., Smoot G.F., Stompor R., Winant C.D., Wu J.H.P., 2000, submitted to ApJ Let. (astro-ph/0005124).
- Bennett, C. L.; Banday, A. J.; Gorski, K. M.; Hinshaw, G.; Jackson, P.; Keegstra, P.; Kogut, A.; Smoot, G. F.; Wilkinson, D. T.; Wright, E. L., 1996, ApJ, 464, L1.
- P. de Bernardis, P.A.R.Ade, J.J.Bock, J.R.Bond, J.Borrill, A. Boscaleri, K.Coble, B.P.Crill, G.De Gasperis, P.C.Farese, P.G.Ferreira, K.Ganga, M.Giacometti, E.Hivon, V.V.Hristov, A.Iacoangeli, A.H.Jaffe, A.E.Lange, L.Martinis, S.Masi, P.Mason, P.D.Mauskopf, A.Melchiorri, L.Miglio, T.Montroy, C.B.Netterfield, E.Pascale, F.Piacentini, D.Pogosyan, S.Prunet, S.Rao, G.Romeo, J.E.Ruhl, F.Scaramuzzi, D.Sforna, N.Vittorio, 2000, 404, 955-959.
- Bertschinger, E. 1987, ApJ, 323, L103.
- Borgani, S., da Costa, L.N., Zehavi, I., Giovanelli, R., Haynes, M., Freudling, W., Wegner G., Salzer, J. J., 2000a, AJ, 119, 102.
- Borgani *et al.* 2000b, in preparation
- Branchini, E.; Teodoro, L.; Trenk, C. S.; Schmoldt, I.; Efstathiou, G.; White, S. D. M.; Saunders, W.; Sutherland, W.; Rowan-Robinson, M.; Keeble, O.; Tadros, H.; Maddox, S.; Oliver, S., 1999, MNRAS, 308, 1
- Burles, S., & Tytler, D., 1998, ApJ, 507, 732
- power spectra measured from redshift catalogs da Costa *et al.* 1996
- da Costa, L.N, Bernardi, M, Alonso, M.V., Wegner, G., Willmer, C.N.A., Pellegrini, P.S., Maia, M.A.G., & Zaroubi, S., 2000a, submitted to ApJ Letters (astro-ph/9912225)
- da Costa, L. N., Bernardi, M., Alonso, M. V., Wegner, G., Willmer, C. N. A., Pellegrini, P. S., Rit e, C., & Maia, M. A. G. 2000b, AJ, submitted.
- da Costa, L.N., Freudling, W., Wegner, G., Giovanelli, R., Haynes, M.P., & Salzer, J.J. 1996, ApJL, 468, L5
- da Costa, L. N., Nusser, A., Freudling, W., Giovanelli, R., Haynes, M. P., Salzer, J. J., & Wegner, G. 1998, MNRAS, 299, 425.
- Davis, M., Nusser, A., & Willick, J.A. 1996, ApJ, 473, 22
- Dekel A. 1994, ARAA, 32, 371

- Efstathiou G., Bond J.R. & White S.D.M., 1992, MNRAS, 258, 1p
- Efstathiou, G.; Bridle, S. L.; Lasenby, A. N.; Hobson, M. P.; Ellis, R. S., 1999, MNRAS, 330, L47.
- Fisher, K.B., Lahav, O., Hoffman, Y., Lynden-Bell, D., & Zaroubi, S. 1995, MNRAS, 272, 885
- Freudling, W., Zehavi, I., da Costa, L.N., Dekel, A., Eldar, A., Giovanelli, R., Haynes, M.P., Salzer, J.J., Wegner, G., & Zaroubi, S. 1999, ApJ, 523, 1.
- Geller, M. J., & Huchra, J. P. 1983, ApJS, 52, 61
- Giovanelli, R.; Haynes, M. P.; Freudling, W.; Da Costa, L. N.; Salzer, J.J.; Wegner, G., 1998, ApJ, 505, L91
- Górski, K.M. 1988, ApJ, 332, L7
- Groth, E. J., Juszkiewicz, R., & Ostriker, J. P. 1989, ApJ, 346, 558
- Hanany S., P. Ade, A. Balbi, J. Bock, J. Borrill, A. Boscaleri, P. de Bernardis, P. G. Ferreira, V. V. Hristov, A. H. Jaffe, A. E. Lange, A. T. Lee, P. D. Mauskopf, C. B. Netterfield, S. Oh, E. Pascale, B. Rabii, P. L. Richards, G. F. Smoot, R. Stompor, C. D. Winant, J. H. P. Wu, 2000, submitted to ApJL. (astro-ph/0005123).
- Hoffman, Y., 1998a, in "Wide Field Surveys in Cosmology", eds. S.Colombi, Y. Mellier and B. Raban (Editions Frontieres), p. 105
- Hoffman, Y., 1998b, to appear in the proceedings of "Evolution of Large Scale Structure – Garching, eds. A.J. Bandy, R.K. Sheth and L.N. da Costa (PrintPartners Ipskamp), p. 148
- Hoffman, Y. & Ribak, E. 1991, ApJL, 380, L5
- Hoffman, Y. Eldar, A., Zaroubi, S., Dekel, A., 2000, preprint.
- Hoffman, Y. and Zaroubi, S., 2000, ApJL (in press, astro-ph/0003306)
- Haynes, M. P. *et al.* 1998, in preparation
- Jaffe, A. H. & Kaiser N., 1995, ApJ, 455, 26.
- Kaiser, N., 1987, MNRAS, 227, 1.
- Kaiser, N. & Stebbins, A. 1991, in *Large Scale Structure and Peculiar Motions in the Universe*, eds. D.W. Latham & L.N. da Costa (ASP Conference Series), p. 111
- Lahav, O., Fisher, K.B., Hoffman, Y., Scharf, C.A., & Zaroubi, S. 1994, ApJL, 423, L93
- A.E. Lange, P.A.R. Ade, J.J. Bock, J.R. Bond, J. Borrill, A. Boscaleri, K. Coble, B.P. Crill, P. de Bernardis, P. Farese, P. Ferreira, K. Ganga, M. Giacometti, E. Hivon, V.V. Hristov, A. Iacangelo, A.H. Jaffe, L. Martinis, S. Masi, P.D. Mauskopf, A. Melchiorri, T. Montroy, C.B. Netterfield, E. Pascale, F. Piacentini, D. Pogosyan, S. Prunet, S. Rao, G. Romeo, J.E. Ruhl, F. Scaramuzzi, D. Sforna, 2000, Submitted to ApJL (astro-ph/0005004)
- Lynden-Bell, D., Faber, S. M., Burstein, D., Davies, R. L., Dressler, A., Terlevich, R., & Wegner, G. 1988, ApJ, 326, 19.
- Maia, M. A. G., da Costa, L. N., & Latham, D. W. 1989, ApJS, 69, 809
- Perlmutter, S.; Aldering, G.; Goldhaber, G.; Knop, R. A.; Nugent, P.; Castro, P. G.; Deustua, S.; Fabbro, S.; Goobar, A.; Groom, D. E.; Hook, I. M.; Kim, A. G.; Kim, M. Y.; Lee, J. C.; Nunes, N. J.; Pain, R.; Pennypacker, C. R.; Quimby, R.; Lidman, C.; Ellis, R. S.; Irwin, M.; McMahon, R. G.; Ruiz-Lapuente, P.; Walton, N.; Schaefer, B.; Boyle, B. J.; Filippenko, A. V.; Matheson, T.; Fruchter, A. S.; Panagia, N.; Newberg, H. J. M.; Couch, W. J.; 1999, ApJ, 517, 565.
- Press, W.H., Teukolsky, S.A., Vetterling, W.T., & Flannery, B.P. 1992, *Numerical Recipes* (Second Edition) (Cambridge: Cambridge University Press)
- Ramella, M., Pisani, A., & Geller, M. J. 1997, AJ, 113, 483.
- Strauss, M.A., & Willick, J.A. 1995, Physics Report, 261, 271
- Sugiyama N., 1995, ApJS, 100, 281
- Sutherland, W.; Tadros, H.; Efstathiou, G.; Frenk, C. S.; Keeble, O.; Maddox, S.; McMahon, R. G.; Oliver, S.; Rowan-
- Robinson, M.; Saunders, W.; White, S. D. M., 1999, MNRAS, 308, 289
- Wegner, G., da Costa L.N., Alonso M. V., Bernardi M., Wilmer C.N.A., Pellegrini P. S., Rite C., Maia M., 2000, Proceedings of the Cosmic Flows workshop, Victoria B.C., Canada, July 1999, eds S. Courteau, M. Strauss, J. Willick, ASP Conference Series.
- Wiener, N. 1949, in *Extrapolation and Smoothing of Stationary Time Series*, (New York: Wiley)
- Willick, J. A., Courteau, S., Faber, S. M., Burstein, D., Dekel, A., & Strauss, M. A. 1997, ApJS, 109, 333
- Zaroubi S. & Hoffman Y., 1996, ApJ, 462, 25.
- Zaroubi, S., Hoffman, Y., Dekel, A., 1999, ApJ, 520, 413.
- Zaroubi, S., Hoffman, Y., Fisher, K.B., & S. Lahav, O. 1995, ApJ, 449, 446
- Zaroubi, S., Zehavi, I., Dekel, A., Hoffman, Y., & Kolatt T., 1997, ApJ, 486, 21
- Zehavi, I., Dekel, A., Nature, 401, 252.